

AllnN for Vertical Power Electronic Devices

Matthew R. Peart¹, Nelson Tansu, *Senior Member, IEEE*,
and Jonathan J. Wierer¹, Jr., *Senior Member, IEEE*

Abstract—The known benefits and challenges of AllnN as a next-generation power electronic semiconductor are presented. $\text{Al}_x\text{In}_{1-x}\text{N}$ is lattice matched to GaN at $x = 0.82$ and has the advantages of an available substrate, a wide bandgap (~ 4.4 eV), and high mobility (~ 450 $\text{cm}^2/\text{V}\cdot\text{s}$). The power figure of merit (FOM), determined using empirical and theoretical values of mobility and estimated critical electric fields determined from reported bandgaps, spans from $\sim 20\%$ to 130% times greater than GaN. In order to realize and precisely determine these high AllnN FOM values, experimental challenges will need to be overcome such as polarization-induced electric fields and bandgap discontinuities at AllnN/GaN interfaces, and controlling carrier concentration levels.

Index Terms—AllnN, GaN, power electronic devices, power figure of merit (FOM), vertical power diodes.

I. INTRODUCTION

WIDE-BANDGAP semiconductors, such as SiC [1] and GaN [2]–[4], are of interest for high figure-of-merit (FOM) power electronic devices to replace Si [5]. The wide bandgap enables power devices with high breakdown voltage, high operating electric fields, high operating temperature, high switching frequency, low switching losses, and an overall higher power FOM. Such devices enable a reduction of the size, weight, and power consumption of electrical systems. Indeed, wide-bandgap SiC and GaN power devices have progressed into viable alternatives with commercial products now replacing some Si-based power devices. There are other less developed semiconductors such as AlGaN and Ga_2O_3 with even wider bandgaps than GaN and SiC that are also interesting for power devices [5]. Power devices based on AlGaN and Ga_2O_3 have great potential but are currently limited because of unavailability of a lattice-matched substrate and no reliable method for p-type doping, respectively. These limitations represent exciting research questions, but no clear solutions exist.

Another possible candidate that, up till now, has been unexplored for future power electronic devices is AllnN.

Manuscript received July 24, 2018; accepted August 20, 2018. Date of publication August 30, 2018; date of current version September 20, 2018. This work was supported by the Lehigh University's Accelerator Program. The review of this paper was arranged by Editor A. Haque. (Corresponding author: Matthew R. Peart.)

The authors are with the Department of Electrical and Computer Engineering, Lehigh University, Bethlehem, PA 18015 USA, and also with the Center for Photonics and Nanoelectronics, Lehigh University, Bethlehem, PA 18015 USA (e-mail: mrp211@lehigh.edu; tansu@lehigh.edu; jwierer@lehigh.edu).

Color versions of one or more of the figures in this paper are available online at <http://ieeexplore.ieee.org>.

Digital Object Identifier 10.1109/TED.2018.2866980

AllnN has a significantly wider bandgap than GaN and therefore can be classified as an ultrawide-bandgap material [5]. Of interest here is $\text{Al}_x\text{In}_{1-x}\text{N}$ that is lattice matched to GaN ($x = 0.82$) [6] and with a bandgap of ~ 4.4 eV. Most research on AllnN has capitalized on this lattice-match property to create AllnN/GaN distributed Bragg reflectors [7], [8], high-electron-mobility transistors [9], [10], Schottky diodes for ultraviolet detection [11], [12], integration as barriers in quantum-well LEDs [13], and thermoelectricity [14], [15]. At this lattice constant and bandgap, it also has many benefits that make it attractive for power electronic devices such as a reasonably high mobility (~ 450 $\text{cm}^2/\text{V}\cdot\text{s}$) [15] and the ability to dope both p-type and n-type [16]. Of course, there are also challenges that need to be overcome such as overcoming polarization fields and bandgap discontinuities at GaN/AllnN heterointerfaces, and controlling carrier concentration levels.

This paper is an early investigation into AllnN semiconductors as a new direction beyond GaN and SiC for power electronic devices. First, the power FOM is determined using best-known physics in order to compare with existing wide-bandgap semiconductors. This includes using simple analytical formulas, and the Silvaco Atlas [17] technology computer-aided design (TCAD) simulator to account for polarization fields and band offsets. As expected, AllnN has a higher FOM than GaN that ranges between $\sim 20\%$ and 130% depending on the values used. Also, the benefits and experimental challenges to realize AllnN power devices, as well as comparisons with AlGaN and Ga_2O_3 , are discussed.

II. MATERIAL PARAMETERS AND FIGURE OF MERIT

The most common way to compare the breakdown voltage and forward resistance properties across power semiconductors is the Baliga FOM [18] expressed as

$$\text{FOM} = \frac{V_b^2}{R_{\text{ON}}} = \frac{\epsilon \mu_n E_c^3}{4} \quad (1)$$

where V_b is the breakdown voltage, R_{ON} is the specific forward (ON) resistance, μ_n is the mobility of the drift layer, and E_c is the critical electric field which includes the effects of impact ionization and avalanche. In general, a higher bandgap leads to higher critical electric fields and a higher FOM; however, this should not be at the detriment of lower mobilities and a higher R_{ON} . To determine the FOM of $\text{Al}_{0.18}\text{In}_{0.82}\text{N}$, the values of E_c and μ_n are taken from theoretical Monte Carlo simulations [19] and also from experimental data [15].

For the $\text{Al}_{0.18}\text{In}_{0.82}\text{N}$ theoretical values, two extreme data sets are used from [19] to provide values for E_c and μ_n .

TABLE I
THEORETICAL AND EXPERIMENTAL VALUES FOR $\text{Al}_{0.82}\text{In}_{0.18}\text{N}$

Parameter set	E_c (MV/cm)	μ_n (cm^2/Vs)	FOM (GW/cm^2)	Ref.
MC alloy scattering	7.6	175	16.42	[19]
MC no alloy scattering	5.1	800	22.68	[19]
Empirical	7.0	450	32.99	[15],[21]

The first set assumes full alloy scattering that results from the total disorder of the $\text{Al}_{0.18}\text{In}_{0.82}\text{N}$ lattice, and the second set is for a totally ordered lattice without alloy scattering. This is different from pure elemental semiconductors without alloy scattering and binary III–V compound semiconductors where alloy scattering is minimal, and causes the analysis of ternary compounds to be more difficult. In reality, the final parameters for $\text{Al}_{0.18}\text{In}_{0.82}\text{N}$ can be expected to fall between these scattering extremes and should be dependent on variables such as growth conditions and defect densities. The result is two sets of ionization rates and mobilities where alloy scattering results in lower mobilities and lower ionization rates.

To determine the critical fields from the Monte Carlo simulations, the ionization rates are converted to fit Chenoweth's model

$$\alpha_e = ae^{-\frac{b}{E}} \quad (2)$$

where α_e is the ionization rate for electrons, a and b are the ionization coefficients, and E is the electric field. For AlInN, the ionization rate for holes is considered negligible as their impact ionization is much lower than electrons at this aluminum composition [19]. This ionization rate model is then used to determine E_c by inputting it into the TCAD simulator for a simple 1-D vertical diode and observing the magnitude of the electric field at the junction during avalanche breakdown.

The empirical FOM values for $\text{Al}_{0.18}\text{In}_{0.82}\text{N}$ are determined the following way. A true experimental value for E_c has yet to be measured, so as an alternative, the measured bandgap (E_g) is used and the critical electric field is estimated using the expression [20]

$$E_c = 1.73 \times 10^5 (E_g)^{2.5} \quad (3)$$

This relationship is derived from a least-squares fit of the known E_c and E_g for various direct bandgap semiconductors and has proven to be relatively accurate for wide-bandgap semiconductors. In fact, for GaN, it slightly underestimates E_c ($\sim 3.7 \text{ MV}/\text{cm}^2$ compared to measured values of $\sim 4 \text{ MV}/\text{cm}^2$ [3]), indicating it is a conservative estimate of the actual value. A value of 4.4 eV is used for E_g for AlInN, as reported by others [21], resulting in an $E_c = 7 \text{ MV}/\text{cm}^2$. An experimental mobility value is used ($450 \text{ cm}^2/\text{V} \cdot \text{s}$) from the published Hall measurement data for n-type AlInN [15].

The summary of critical electric field and mobility values used for $\text{Al}_{0.18}\text{In}_{0.82}\text{N}$ are shown in Table I and are used to determine the FOM and compare to other semiconductors. Fig. 1 shows a plot of R_{ON} versus breakdown voltage for power devices with drift layers comprised SiC, GaN, Ga_2O_3 ,

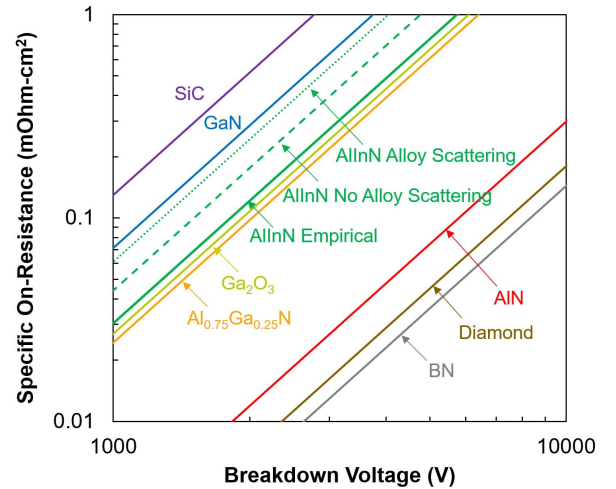


Fig. 1. Specific ON-resistance versus reverse breakdown voltage for SiC, GaN, Ga_2O_3 , $\text{Al}_{0.75}\text{Ga}_{0.25}\text{N}$, AlN, diamond, BN, and theoretical and empirical values of $\text{Al}_{0.82}\text{In}_{0.18}\text{N}$. The FOM becomes higher from the top left to the bottom right. The $\text{Al}_{0.82}\text{In}_{0.18}\text{N}$ has comparable FOM with Ga_2O_3 and $\text{Al}_{0.75}\text{Ga}_{0.25}\text{N}$.

$\text{Al}_{0.75}\text{Ga}_{0.25}\text{N}$, AlN, diamond, and BN using acceptable values for E_c and μ_n [3], [5]. The particular alloy concentration for $\text{Al}_{0.75}\text{Ga}_{0.25}\text{N}$ was chosen, because at this high Al concentration, the mobility is less dominated by alloy scattering and higher FOMs than GaN can be achieved while also having an aluminum concentration low enough that donors are ionized [22]. Fig. 1 also includes the three different theoretical and empirical values for $\text{Al}_{0.18}\text{In}_{0.82}\text{N}$ for comparison. Semiconductors with data on the bottom right of the plot have higher FOM as suggested by (1).

Two distinct groupings are visible in Fig. 1 where group 1 is close to, but at higher FOM than GaN ($\text{Al}_{0.18}\text{In}_{0.82}\text{N}$, Ga_2O_3 , and $\text{Al}_{0.75}\text{Ga}_{0.25}\text{N}$), and the second group with much higher FOM (diamond, AlN, and BN). $\text{Al}_{0.18}\text{In}_{0.82}\text{N}$ has a higher FOM than GaN and potentially could be similar in performance to Ga_2O_3 and $\text{Al}_{0.75}\text{Ga}_{0.25}\text{N}$. The two theoretical values are less than the empirical value, and of course, further work will be necessary to determine the absolute FOM. The second grouping has much larger bandgaps and is approaching insulator properties. The benefits and challenges of the three semiconductors in the first grouping are discussed later because of their similar FOM.

III. TCAD SIMULATION RESULTS

A vertical $\text{Al}_{0.82}\text{In}_{0.18}\text{N}$ power diode is simulated using the Silvaco Atlas TCAD software with the empirical critical electric fields and mobility values shown in Table I. To perform this simulation, E_c is converted into an impact ionization rate using (2), and the mobility is a simple constant value. The TCAD simulation is not expected to reveal a different FOM compared to the analytical solutions but is performed to understand some of the unique challenges of AlInN power devices. For example, it is shown in the following that a conduction band discontinuity across the GaN/AlInN heterointerface causes increased resistance unless it is engineered properly. Other parameters included in the TCAD model are

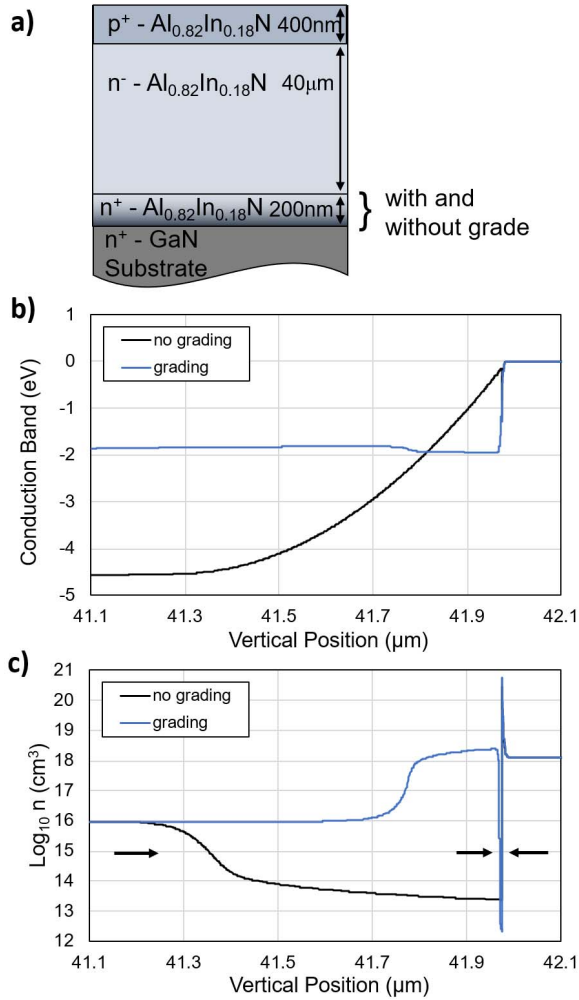


Fig. 2. (a) Cross-sectional schematic of the simulated AlInN power diode. (b) Plots of conduction band energy versus vertical position and (c) carrier concentration (n) versus vertical position for the structures with and without a doping grade at the AlInN/GaN heterointerface and at a forward voltage of 10 V. Arrows: length of the depletion layer thickness.

the spontaneous polarization, bandgaps, dielectric constants, effective masses, and affinities [21], [23], [24].

The simulated structure is shown in Fig. 2(a). The n-type drift layer consists of Al_{0.82}In_{0.18}N that is 40 μm thick and doped with a Si (donor) concentration of 10¹⁶ cm⁻³. This donor concentration calculated by (4) is nearly optimal for a 40-μm-thick drift layer to spread the electric field over its entire length while avoiding punchthrough

$$N_D = \frac{\epsilon E_c}{qW}. \quad (4)$$

The p-type layer consists of Al_{0.82}In_{0.18}N that is 400 nm thick and doped with a Mg (acceptor) concentration of 10¹⁹ cm⁻³. Alternatively, p-type GaN could have been used because it is lattice matched and it could also be a method to ensure ohmic contacts. These layers are formed on a GaN substrate. At the Al_{0.82}In_{0.18}N and GaN heterointerface, there is a bandgap discontinuity, an electron concentration or Fermi level discontinuity, and band bending caused by polarization charges. A conduction band offset ΔE_c of 70% of the bandgap

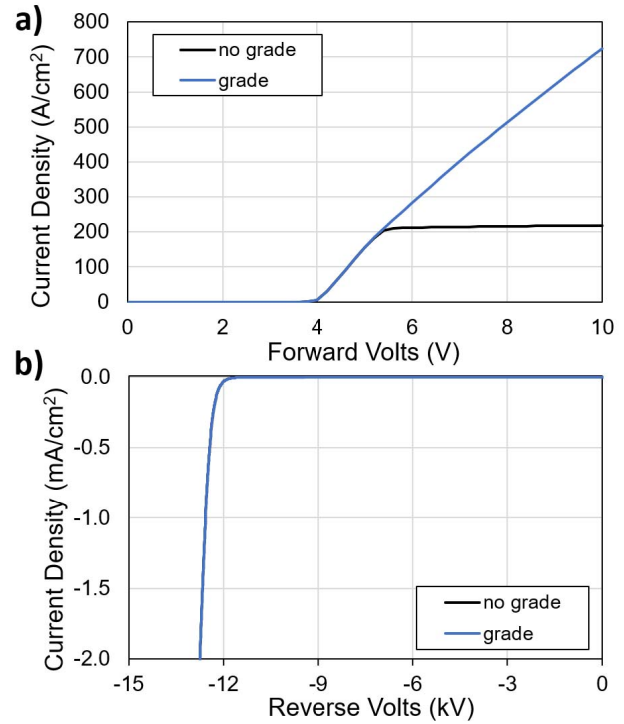


Fig. 3. Plots of current versus (a) forward and (b) reverse voltages for the simulated diodes with and without a doping grade at the AlInN/GaN heterointerface. The doping grade reduces the depletion layer [arrows in Fig. 2(b)] resulting in a lower specific on-resistance. The reverse breakdown voltage is ~13 kV.

offset is used [21] although this value varies from 60% to 90% in various reports.

There is a unipolar n⁺/n⁻ junction at the AlInN/GaN heterointerface that is in series but in the opposite in polarity to the main p-n junction. When the entire structure is biased such that the main p-n junction is in the forward bias, the n⁺/n⁻ heterojunction is in the reverse bias. At a high enough voltage, the heterojunction dominates the resistance and limits current. Fig. 2(b) and (c) shows the conduction band energy and carrier concentration versus vertical position at the GaN/AlInN heterointerface and a forward bias of 10 V. For the structures without a doping grade (black line), the conduction band bends over a long distance (~600 nm), resulting a low carrier concentration depletion (or space charge) layer. This depletion layer represents the high resistance in series with the forward-biased p-n junction. To overcome this detrimental resistance, a doping grade is used that begins at the heterointerface at a donor concentration of 5 × 10¹⁹ cm⁻³ and terminates 200 nm into the Al_{0.82}In_{0.18}N down to the drift doping level of 10¹⁶ cm⁻³. This doped structure greatly reduces the length of the band bending, the thickness of the depletion layer, and the resistance.

The resultant current versus voltage (IV) characteristics of both structures is shown in Fig. 3(a) and (b) for the forward bias and the reverse bias, respectively. The diode without the doping grade has an I - V characteristic with two different resistance regimes. At the lowest currents, the resistance is comparable to the structure with the graded doping

TABLE II

COMPARISON OF SEMICONDUCTORS WITH COMPARABLE FOM

Property	GaN	Al _{0.82} In _{0.18} N	β -Ga ₂ O ₃	Al _{0.75} Ga _{0.25} N
Bandgap (eV)	3.4	4.4	4.9	5.3
Critical electric field (MV/cm)	3.9	7	10	11
Lattice Matched Substrate	Yes	Yes	Yes	No
Demonstrated p-type doping	Good	Moderate	No	Poor
Demonstrated n-type doping	Good	Good	Good	Moderate
Mobility (cm ² /Vs)	1100	450	153	150
Thermal conductivity (W/mK)	253	5	11-27	30

($\sim 14 \text{ m}\Omega \cdot \text{cm}^2$), but at higher bias, the depleted resistive layer increases and finally dominates the forward resistance with $R_{\text{ON}} \sim 46 \text{ m}\Omega \cdot \text{cm}^2$. The graded doping mostly corrects the heterointerface resistance. If one uses even lower conduction band discontinuities, then the resistance improves (data not show) and is solely due to the drift layer which is $\sim 5.5 \text{ m}\Omega \cdot \text{cm}^2$. This doping scheme is far from optimized and only highlights the problem and potential solutions. For example, the resistance could be further reduced by other means such as using an AlGaN interlayer or alloy grading.

The reverse bias performance for both structures is the same because when the p-n junction is in the reverse bias, the unipolar AlInN/GaN heterointerface is forward biased. Fig. 3(b) shows a reverse breakdown of $\sim 13 \text{ kV}$ for both structures that are consistent with the high critical electric field for AlInN. As a comparison, a power diode with a GaN drift layer of the same thickness and doping has a reverse breakdown of $\sim 4 \text{ kV}$. Of course, this breakdown voltage is a function of the drift layer thickness and doping, and higher breakdown voltages are possible.

IV. DISCUSSION OF BENEFITS AND CHALLENGES

It will take some experimental work to overcome some unique challenges and realize these impressive FOM values for AlInN. Table II highlights the benefits and challenges of AlInN compared to other ultrawide-bandgap semiconductors in the same class. The discussion is limited to the first band of semiconductors shown in Fig. 1 with higher FOM than GaN and similar bandgaps (Al_{0.82}In_{0.18}N, Al_{0.75}Ga_{0.25}N, and Ga₂O₃). The semiconductors in the second higher grouping have far greater bandgaps that are approaching insulating characteristics and are not discussed. They also have more difficult challenges in doping and growth although there has been significant progress with diamond [5].

The primary advantage of AlInN is it can be lattice matched to GaN. With the availability of GaN substrates, this enables vertical AlInN devices and the ability to create thick drift layers without creating dislocations that can occur from lattice-mismatched growth. It is the availability of substrates for any semiconductor that is a huge barrier to realize vertical power devices, and substrate availability has, for example, generated a lot of research on GaN and Ga₂O₃ for power devices [5], [25], [26]. This is clearly an advantage over Al_{0.75}Ga_{0.25}N which has to be grown on nonconductive AlN,

GaN, or SiC, all of which are highly lattice mismatched. There has been some work on AlGaN power devices that use patterning and regrowth to compensate for the lattice-mismatched growth [27], but the dislocation densities are still higher than those of lattice-matched growth.

Another benefit of Al_{0.82}In_{0.18}N is the ability to dope both n-type and p-type. [21] Again, this is an advantage over Al_{0.75}Ga_{0.25}N and Ga₂O₃, both of which have demonstrated low or no p-type conductivity. For Al_{0.75}Ga_{0.25}N, polarization doping can possibly be used [27], [28], but this limits layer thicknesses to the hundreds of nanometers. The ability to complimentary dope Al_{0.82}In_{0.18}N means that one can more easily create three-terminal devices such as field-effect transistors or bipolar junction transistors. However, one possible challenge is if selective doping (via implantation, diffusion, or regrowth) can be achieved in Al_{0.82}In_{0.18}N without compromised interfaces, because this is a problem that currently has not been overcome in GaN.

Alternatively, p-type GaN layers could also be used although band bending due to spontaneous polarization needs to be considered in any device design. However, this also raises the intriguing possibility to create vertical power devices with GaN/AlInN heterointerfaces. Although outside the scope of this discussion, there is the possibility of capitalizing on polarization doping (using lattice-matched and graded composition AlInGaN) or forming channels as done in AlN/GaN high-electron-mobility transistors (HEMTs) [9], [28].

Another major challenge in doping Al_{0.82}In_{0.18}N will be the ability to control carrier concentration levels. Measured electron concentrations are typically high $> 5 \times 10^{17} \text{ cm}^{-3}$ [6], [29], and hole concentrations are low $\sim 5 \times 10^{15} \text{ cm}^{-3}$ [16], [29]. It is known that there is a high concentration of oxygen in the films that most likely behave as an n-type dopant [29] that limits the concentrations of electrons and holes. Experiments are necessary to identify and remove these compensating mechanisms. Even with high compensation, Al_{0.82}In_{0.18}N has been able to achieve high experimental electronic mobilities that even in the presence of alloy, scattering is higher than Al_{0.75}Ga_{0.25}N and Ga₂O₃ [15].

All three semiconductors in this class have lower thermal conductivity compared to binary and elemental semiconductors. Current-known values place AlInN slightly lower than Al_{0.75}Ga_{0.25}N and Ga₂O₃. However, the experimental work to produce these AlInN films were designed to have low thermal conductivity for thermoelectricity applications [15]. There is a possibility that experimentation focused on reducing alloy scattering will produce higher thermal conductivities. Also, AlInN has the benefit of being able to be grown on higher conductivity GaN substrates which could also help with thermal dissipation.

Previous reports have identified gate leakage as an issue in AlInN/GaN HEMTs [31]–[33]. These HEMTs are grown on high dislocation GaN/sapphire templates and consist of thin AlInN layers. One could expect leakage in other AlInN devices, but most of these leakage mechanisms should not negatively affect the performance in vertical AlInN power devices grown on low dislocation substrates with thick AlInN drift layers. For example, leakage due to tunneling [31], [32] is

not of concern in thick drift layers, and space-charge leakage caused by dislocations [32] should be minimized on bulk GaN substrates.

Finally, there are some other challenges that are of concern for AlInN mostly because power devices have never been attempted in this material system. One potential challenge that has yet to be demonstrated is the growth of thick (tens of micrometer) drift layers where lattice matching and carrier concentration are maintained for vertical devices. In addition, these drift layers will require fast growth rates for ease of manufacturability, and in fact, high growth rates at $0.9 \mu\text{m/h}$ have been demonstrated [34], which should allow for the exploration of thick AlInN drift layers until faster growth rates are achieved. In fact, this paper will also motivate experiments on high growth rates of AlInN. Prior work did not identify this as a specific need as the primary structures were based on the nanoscale and thin-film structures. Finally, just as with other power devices, edge termination schemes [35], [36] will need to be developed to realize high breakdown voltages.

V. CONCLUSION

The benefits and challenges of AlInN as a next-generation power electronic semiconductor are presented. $\text{Al}_{0.82}\text{In}_{0.18}$ has an FOM that exceeds that of GaN and be competitive with $\text{Al}_{0.75}\text{Ga}_{0.25}\text{N}$ and Ga_2O_3 . It also has additional benefits such as a lattice match substrate, the ability to dope n-type and p-type, and high electron mobilities. The advantages of AlInN elucidated here should motivate further interest to tackle the challenges faced in this material for power electronic applications.

REFERENCES

- [1] B. A. Hull *et al.*, "Performance and stability of large-area 4H-SiC 10-kV junction barrier Schottky rectifiers," *IEEE Trans. Electron Devices*, vol. 55, no. 8, pp. 1864–1870, Aug. 2008, doi: [10.1109/TED.2008.926655](#).
- [2] I. C. Kizilyalli, A. P. Edwards, H. Nie, D. Bour, T. Prunty, and D. Disney, "3.7 kV vertical GaN PN diodes," *IEEE Electron Device Lett.*, vol. 35, no. 2, pp. 247–249, Feb. 2014, doi: [10.1109/LED.2013.2294175](#).
- [3] A. M. Armstrong *et al.*, "High voltage and high current density vertical GaN power diodes," *Electron. Lett.*, vol. 52, no. 13, pp. 1170–1171, Jun. 2016, doi: [10.1049/el.2016.1156](#).
- [4] I. C. Kizilyalli, A. P. Edwards, H. Nie, D. Disney, and D. Bour, "High voltage vertical GaN p-n diodes with avalanche capability," *IEEE Trans. Electron Devices*, vol. 60, no. 10, pp. 3067–3070, Oct. 2013, doi: [10.1109/TED.2013.2266664](#).
- [5] J. Y. Tsao *et al.*, "Ultrawide-bandgap semiconductors: Research opportunities and challenges," *Adv. Electron. Mater.*, vol. 4, no. 1, p. 1600501, 2018, doi: [10.1002/aem.201600501](#).
- [6] G. Liu *et al.*, "Metalorganic vapor phase epitaxy and characterizations of nearly-lattice-matched AlInN alloys on GaN/sapphire templates and free-standing GaN substrates," *J. Cryst. Growth*, vol. 340, no. 1, pp. 66–73, 2012, doi: [10.1016/j.jcrysgro.2011.12.037](#).
- [7] J.-F. Carlin and M. Ilegems, "High-quality AlInN for high index contrast Bragg mirrors lattice matched to GaN," *Appl. Phys. Lett.*, vol. 83, no. 4, pp. 668–670, 2003, doi: [10.1063/1.1596733](#).
- [8] M. M. Satter *et al.*, "Design and analysis of 250-nm AlInN laser diodes on AlN substrates using tapered electron blocking layers," *IEEE J. Quantum Electron.*, vol. 48, no. 5, pp. 703–711, May 2012, doi: [10.1109/JQE.2012.2190496](#).
- [9] E. Kohn and F. Medjdoub, "InAlN—A new barrier material for GaN-based HEMTs," in *Proc. 14th Int. Workshop Phys. Semiconductor Devices (IWPSD)*, vol. 6, Dec. 2007, pp. 311–316, doi: [10.1109/IWPSD.2007.4472506](#).
- [10] Q. Fareed, A. Tarakji, J. Dion, M. Islam, V. Adivarahan, and A. Khan, "High voltage operation of field-plated AlInN HEMTs," *Phys. Status Solidi Current Topics Solid State Phys.*, vol. 8, nos. 7–8, pp. 2454–2456, 2011, doi: [10.1002/pssc.201001103](#).
- [11] Y. Sakai, T. Morimoto, T. Egawa, and T. Jimbo, "Metal organic chemical vapor deposition growth and characterization of AlInN-based Schottky ultraviolet photodiodes on AlN template," *Jpn. J. Appl. Phys.*, vol. 50, p. 01AD01, Jan. 2011, doi: [10.1143/JJAP.50.01AD01](#).
- [12] Z. T. Chen, S. X. Tan, Y. Sakai, and T. Egawa, "Improved performance of InAlN-based Schottky solar-blind photodiodes," *Appl. Phys. Lett.*, vol. 94, no. 21, p. 213504, 2009, doi: [10.1063/1.3142870](#).
- [13] W. Sun, S. A. Al Mueyed, R. Song, J. J. Wierer, Jr., and N. Tansu, "Integrating AlInN interlayers into InGaN/GaN multiple quantum wells for enhanced green emission," *Appl. Phys. Lett.*, vol. 112, no. 20, p. 201106, 2018, doi: [10.1063/1.5028257](#).
- [14] J. Zhang, S. Kutlu, G. Liu, and N. Tansu, "High-temperature characteristics of Seebeck coefficients for AlInN alloys grown by metalorganic vapor phase epitaxy," *J. Appl. Phys.*, vol. 110, no. 4, p. 043710, 2011, doi: [10.1063/1.3624761](#).
- [15] J. Zhang, H. Tong, G. Liu, J. A. Herbsommer, G. S. Huang, and N. Tansu, "Characterizations of seebeck coefficients and thermoelectric figures of merit for AlInN alloys with various in-contents," *J. Appl. Phys.*, vol. 109, no. 5, p. 053706, 2011, doi: [10.1063/1.3553880](#).
- [16] Y. Taniyasu, J.-F. Carlin, A. Castiglia, R. Butté, and N. Grandjean, "Mg doping for p-type AlInN lattice-matched to GaN," *Appl. Phys. Lett.*, vol. 101, no. 8, p. 082113, 2012, doi: [10.1063/1.4747524](#).
- [17] *Silvaco Atlas TCAD*, Silvaco, Santa Clara, CA, USA, 2016.
- [18] B. J. Baliga, *Fundamentals of Power Semiconductor Devices*. New York, NY, USA: Springer, 2008.
- [19] S. Shishehchi, F. Bertazzi, and E. Bellotti, "A numerical study of low- and high-field carrier transport properties in $\text{In}_{0.18}\text{Al}_{0.82}\text{N}$ lattice-matched to GaN," *J. Appl. Phys.*, vol. 113, no. 20, p. 203709, 2013, doi: [10.1063/1.4807914](#).
- [20] J. L. Hudgins, G. S. Simin, E. Santi, and M. A. Khan, "An assessment of wide bandgap semiconductors for power devices," *IEEE Trans. Power Electron.*, vol. 18, no. 3, pp. 907–914, May 2003, doi: [10.1109/TPEL.2003.810840](#).
- [21] R. Butté *et al.*, "Current status of AlInN layers lattice-matched to GaN for photonics and electronics," *J. Phys. D, Appl. Phys.*, vol. 40, no. 20, pp. 6328–6344, 2007, doi: [10.1088/0022-3727/40/20/S16](#).
- [22] M. E. Coltrin and R. J. Kaplar, "Transport and breakdown analysis for improved figure-of-merit for AlGaIn power devices," *J. Appl. Phys.*, vol. 121, no. 5, p. 055706, 2017, doi: [10.1063/1.4975346](#).
- [23] J. Piprek, *Nitride Semiconductor Devices: Principles and Simulation*. Weinheim, Germany: Wiley, 2007.
- [24] S. L. Chuang, *Physics of Photonic Devices*, 2nd ed. Hoboken, NJ, USA: Wiley, 2009.
- [25] S. J. Pearton *et al.*, "A review of Ga_2O_3 materials, processing, and devices," *Appl. Phys. Rev.*, vol. 5, no. 1, p. 011301, 2018, doi: [10.1063/1.5006941](#).
- [26] J. Millan, P. Godignon, X. Perpina, A. Perez-Tomas, and J. Rebollo, "A survey of wide bandgap power semiconductor devices," *IEEE Trans. Power Electron.*, vol. 29, no. 5, pp. 2155–2163, May 2014, doi: [10.1109/TPEL.2013.2268900](#).
- [27] A. A. Allerman *et al.*, " $\text{Al}_{0.3}\text{Ga}_{0.7}\text{N}$ PN diode with breakdown voltage > 1600 V," *Electron. Lett.*, vol. 52, no. 15, pp. 1319–1321, 2016, doi: [10.1049/el.2016.1280](#).
- [28] D. Jena *et al.*, "Polarization-engineering in group III-nitride heterostructures: New opportunities for device design," *Phys. Status Solidi A*, vol. 208, no. 7, pp. 1511–1516, Jul. 2011, doi: [10.1002/pssa.201001189](#).
- [29] M. A. Py, L. Lugani, Y. Taniyasu, J.-F. Carlin, and N. Grandjean, "Capacitance behavior of InAlN Schottky diodes in presence of large concentrations of shallow and deep states related to oxygen," *J. Appl. Phys.*, vol. 117, no. 18, p. 185701, 2015, doi: [10.1063/1.4919846](#).
- [30] E. Bellotti and F. Bertazzi, "A numerical study of carrier impact ionization in $\text{Al}_x\text{Ga}_{1-x}\text{N}$," *J. Appl. Phys.*, vol. 111, no. 10, p. 103711, 2012, doi: [10.1063/1.4719967](#).
- [31] E. Arslan, S. Altundal, S. Özçelik, and E. Ozbay, "Tunneling current via dislocations in Schottky diodes on AlInN/AlN/GaN heterostructures," *Semicond. Sci. Technol.*, vol. 24, no. 7, p. 075003, 2009.
- [32] S. Ganguly, A. Konar, Z. Hu, H. Xing, and D. Jena, "Polarization effects on gate leakage in InAlN/AlN/GaN high-electron-mobility transistors," *Appl. Phys. Lett.*, vol. 101, no. 25, pp. 253519–1–253519-3, Dec. 2012.

- [33] S. Turuvekere, N. Karumuri, A. A. Rahman, A. Bhattacharya, A. Dasgupta, and N. DasGupta, "Gate leakage mechanisms in AlGaIn/GaN and AlInN/GaN HEMTs: Comparison and modeling," *IEEE Trans. Electron Devices*, vol. 60, no. 10, pp. 3157–3165, Oct. 2013.
- [34] A. V. Lobanova, A. S. Segal, E. V. Yakovlev, and R. A. Talalaev, "AlInN MOVPE: Growth chemistry and analysis of trends," *J. Cryst. Growth*, vol. 352, no. 1, pp. 199–202, Aug. 2012, doi: [10.1016/j.jcrysgro.2011.11.015](https://doi.org/10.1016/j.jcrysgro.2011.11.015).
- [35] J. J. Wierer, J. R. Dickerson, A. A. Allerman, A. M. Armstrong, M. H. Crawford, and R. J. Kaplar, "Simulations of junction termination extensions in vertical GaN power diodes," *IEEE Trans. Electron Devices*, vol. 64, no. 5, pp. 2291–2297, May 2017, doi: [10.1109/TED.2017.2684093](https://doi.org/10.1109/TED.2017.2684093).
- [36] J. R. Dickerson *et al.*, "Vertical GaN power diodes with a bilayer edge termination," *IEEE Trans. Electron Devices*, vol. 63, no. 1, pp. 419–425, Jan. 2016, doi: [10.1109/TED.2015.2502186](https://doi.org/10.1109/TED.2015.2502186).



Matthew R. Peart received the B.S. degree in electrical engineering from Villanova University, Villanova, PA, USA, and the M.S. degree in electrical engineering from Lehigh University, Bethlehem, PA, USA, where he is currently pursuing the Ph.D. degree.

He held research and development positions with Intel, Hillsboro, OR, USA, and Broadcom Limited, Breinigsville, PA, USA. His current research interests include III-nitride device physics and numerical simulation.



Nelson Tansu (SM'09) received the B.S. degree in applied mathematics, electrical engineering, and physics, and the Ph.D. degree in electrical engineering from the University of Wisconsin–Madison, Madison, WI, USA, in 1998 and 2003, respectively.

He is currently the Daniel E.'39 and Patricia M. Smith Endowed Chair Professor with the Department of Electrical and Computer Engineering, Lehigh University, Bethlehem, PA, USA.



Jonathan J. Wierer, Jr. (M'95–SM'12) received the B.S., M.S., and Ph.D. degrees in electrical engineering from the University of Illinois, Urbana–Champaign, IL, USA, in 1994, 1995, and 1999, respectively.

He was with Philips-Lumileds, San Jose, CA, USA, and Sandia National Laboratories, Albuquerque, NM, USA. He is currently an Associate Professor with Lehigh University, Bethlehem, PA, USA. He has authored or co-authored over 150 publications and conference publications, and holds 37 patents.